Sensitivity and resolution in noncontact electrostatic force microscopy in the case of a constant potential

G. Lévêque,* P. Cadet, and R. Arinero
LAIN, Laboratoire d'Analyse des Interfaces et de Nanophysique, UMR CNRS 5011, Université Montpellier II, Sciences et Techniques du Languedoc, Place Eugène Bataillon, CC 082, 34095 Montpellier Cedex 5, France
(Received 1 December 2004; published 27 May 2005)

The basic dynamic equations of the electrostatic force microscope are derived, in the case of a constant potential applied to a spherical tip above a conducting plane sample. The microscope tip moves in the electrostatic field, providing a force supposed to be inversely proportional to the distance. The linear and nonlinear approximations are treated to obtain the amplitude and phase of the vibration, at a fixed frequency. Optimal experiment conditions, i.e., distance, frequency, and voltage, which give the best sensitivity and lateral resolution, are discussed. The stability of the oscillations during the scans is dependent on the experiment conditions. In addition to the tapping regime, we show that two stable noncontact regimes may exist in some conditions. Only one stable noncontact oscillation occurs at a working frequency equal or superior to the natural frequency of the system. When a distance equal to the free amplitude is selected, the phase shift due to the potential is linear in function of the applied potential (instead of quadratic as observed at larger distances) and a good sensitivity to the potential of the sample is obtained. The theoretical lateral resolution is derived in the linear and nonlinear approximations, and is shown to depend strongly on the mean tip-sample distance. In the examples shown, the best resolution values are reached at a very close distance, with values much lower than the tip apex radius.

DOI: 10.1103/PhysRevB.71.205419 PACS number(s): 68.37.Ps, 07.79.Lh, 81.70.Ex

I. INTRODUCTION

Noncontact atomic force microscopy (NC-AFM) or dynamic force microscopy (DFM) has proven to be an effective method for imaging semiconductor and insulator surfaces up to atomic resolution.[1,2] This result was made possible by vibrating the tip very close to the surface, where short-range interactions are predominant, for instance chemical bonding force[3–6] or electrostatic forces on ionic crystals.[7–9]

When long-range electrostatic forces are used to measure the surface potential and charges, for example for microelectronic device studies,[10–14] one speaks of electrostatic force microscopy (EFM) or Kelvin force microscopy (KFM). In these setups, the tip of the microscope is vibrated at a mean distance of several nanometers. At this distance, the atomic nature of the sample and the tip is smoothed and the media can be considered as continuous. Consequently, an atomic resolution is not expected.

The sensitivity of the experiments and its lateral resolution are directly related to the characteristics of the vibration, namely the driving frequency, the amplitude, the mean distance and the tip voltage, which can be chosen freely by the experimentalist. The aim of the present article is to provide the basic clues to obtain the best sensitivity and resolution in electrostatic force microscopy.

The first evident assumption is that the tip should be vibrated as close as possible to the sample, in order to reduce the extension of the interaction. In this case, the electrostatic force is strongly dependent on the tip sample distance, and $F(d)$ absolutely nonlinear. The basic equation for the motion of a tip in a nonlinear field of force has been widely treated in literature, but mostly applied to Van der Waals forces, decaying in $1/d^2$,[15–19] or to chemical short range interaction.[20,21] Electrostatic force, decreasing in $1/d$, as for sphere-plane geometry, has been less studied.[22–24] Sometimes, a sinusoidal voltage is applied (as in Kelvin force microscopy); this corresponds to a more complex experiment, where the dynamics of the transient phase should be considered.

The sensitivity and lateral resolution for an electrostatic force decreasing in $1/d$ is the only case treated below, because it is considered as an ideal case. In addition, we supposed a constant applied voltage and conducting tip and sample to simplify the problem. The results concern only microscopes driven at constant frequency (amplitude variable during the scans), and not systems with frequency modulation.

II. BASIC DYNAMIC EQUATION

In the noncontact mode, the height of the tip above the sample surface, noted $H(t)$, is always positive. Negative values indicate that contact occurs, (leading to intermittent contact or tapping mode). The penetration of the tip into the sample would induce elastic repulsive forces, which are not considered here.[17]

The mechanical part of the tip-cantilever system is approximated here by a mass-spring system. The electrostatic force applies to a punctual mass fastened to a spring without mass. It has been verified that this approximation is valid for low frequency vibrations, close to the fundamental frequency of the cantilever. In this case, the higher harmonic modes of the beam[25,26] are ignored.

The position $H(t)$ of the mass obeys the following differential equation:

$$mH''(t) + cH'(t) + k(H(t) - h) = F_{elec}(t) + F_{exc}(t), \quad (1)$$

where F_{elec} is the sum of the electrostatic forces applied to the tip+cantilever system, h the position of equilibrium in the absence of any force, and $F_{\text{exc}}(t)$ is the exciting force. $F_{\text{exc}}(t)$ is supposed sinusoidal, with a pulsation ω_{m}, close to the resonance:

$$F_{exc}(t) = F\cos(\omega_m t + \pi/2). \quad (1')$$

The $+\pi/2$ term allows the phase of $H(t)$ to be zero at resonance, far from the sample.

The electrostatic force between a spherical tip (apex radius R) and a plane sample (both conducting) can be calculated. In the case of small distances ($H < R/10$) the asymptotic expression is

$$F_{elec}(t) = -\frac{\pi\varepsilon_0 RV^2}{H(t)}. \quad (2)$$

At larger distances, the force on the conical part of the tip and on the cantilever are not negligible.[27,28] As the complete force expression is too complicated for the following treatments, we choose to consider only an additional constant term "α," to represent the contribution of cantilever and the cone:

$$F_{elec}(t) = -\left[\frac{\pi\varepsilon_0 R}{H(t)} + \alpha\right]V^2. \quad (3)$$

For distances greater than $R/2$, the approximation is probably less satisfying, as discussed later.

With an excitation at pulsation ω_{m}, and a large quality factor Q for the system (for instance $Q=100$ for a microscope operating in air) the response of the system is expected to be nearly sinusoidal:

$$H(t) = h + z(t) = h + z_0 + z_1\cos(\omega_m t + \varphi). \quad (4)$$

z_0 is the constant deflection of the cantilever due to the mean attractive force, and z_1 the vibration amplitude.

Reporting the above expressions in the differential equation, and introducing the free pulsation of the system ω_0, the effective mass $m = k/\omega_0^2$, and the damping factor $c = k/(\omega_0 Q)$ gives

$$\frac{z''(t)}{\omega_0^2} + \frac{z'(t)}{\omega_0 Q} + z(t) = \frac{F_{exc}(t)}{k} - \left[\frac{\pi\varepsilon_0 R}{h + z(t)} + \alpha\right]\frac{V^2}{k}. \quad (5)$$

As it is more convenient to work with reduced values without dimension, we follow below the notation of Ref. 17 and divide the displacements by the maximum vibration amplitude, in the absence of electrostatic force, at $\omega_{\text{m}} = \omega_0$, which is $Z = QF/k$. We introduce the reduced flexion of the cantilever $a_0 = z_0/Z$, the reduced amplitude $a_1 = z_1/Z$, the reduced distance $d = h/Z$, and the reduced pulsation $u = \omega_{\text{m}}/\omega_0$. Expression (5) becomes

$$\frac{a''(t)}{\omega_0^2} + \frac{a'(t)}{\omega_0 Q} + a(t) = \frac{1}{Q}\cos\left(\omega_m t + \frac{\pi}{2}\right) - \frac{\pi\varepsilon_0 RV^2}{kZ^2[d + a(t)]} - \frac{\alpha V^2}{kZ} \quad (6)$$

with $a(t) = z(t)/Z = a_0 + a_1\cos(\omega_m t + \varphi)$.

This expression can be resolved, with three degrees of precision, at the first order (linear approximation), at the second order (called nonlinear approximation), and numerically for full precision results. The three cases are developed below.

A. Linear approximation

The most simple approximation consists in taking the first order polynomial development of the force term $1/(d+a) = 1/d - a/d^2$, approximation which is valid if the flexion is much smaller than the distance $a \ll d$. Developing expression (6) and using $u = \omega_{\text{m}}/\omega_0$ gives

$$(1-u^2)a_1\cos(\omega_m t + \varphi) - \frac{u}{Q}a_1\sin(\omega_m t + \varphi) + a_0 = \frac{1}{Q}\cos\left(\omega_m t + \frac{\pi}{2}\right) - \frac{\pi\varepsilon_0 RV^2}{kZ^2 d^2}[d - a_0 - a_1\cos(\omega_m t + \varphi)] - \frac{\alpha V^2}{kZ}. \quad (7)$$

This equation can be separated into a constant expression, giving a_0,

$$a_0 = -\frac{\pi\varepsilon_0 RV^2}{kZ^2}\frac{d - a_0}{d^2} - \frac{\alpha V^2}{kZ} \quad (8)$$

and a sinusoidal expression, best written in the complex Fresnel notation:

$$\left(1 - u^2 + \frac{iu}{Q}\right)\tilde{a}_1 = \frac{i}{Q} + \frac{\pi\varepsilon_0 RV^2}{kZ^2 d^2}\tilde{a}_1. \quad (9)$$

Using the gradient expression

$$g = \frac{\pi\varepsilon_0 RV^2}{Z^2 d^2}, \quad (10)$$

the complex amplitude is deduced:

$$\tilde{a}_1 = \frac{1}{u - iQ(1 - u^2 - g/k)} \quad (11)$$

or in real notation

$$a_1 = \frac{1}{\sqrt{u^2 + Q^2(1 - u^2 - g/k)^2}} \quad (12)$$

and

$$\varphi = \arctan\left[\frac{Q(1 - u^2 - g/k)}{u}\right] \quad (12')$$

We note also that a relation independent of the electrostatic gradient connects the amplitude and the phase:

$$\cos(\varphi) = ua_1. \tag{13}$$

The gradient of the electrostatic force shifts the resonance of the system towards lower frequencies. The shift, $\Delta u = -g/2k$, is proportional to V^2 and can be used to deduce the sample potential. The above approximation is the classic theory for electrostatic force microscopy, and Kelvin microscopy.

B. Nonlinear approximation

When the amplitude of the vibration is in the same order of magnitude as the distance, the precedent linear approximation is no longer valid. A better approximation is given below, supposing only that $a < d$, to insure a true noncontact mode.

The base of the calculus is to develop the electrostatic force in Fourier series. The electrostatic force in Eq. (6) is developed over the first Fourier harmonics:

$$\frac{1}{d + a_1\cos(\omega_m t + \varphi)} = t_0 + t_1\cos(\omega_m t + \varphi) + \cdots. \tag{14}$$

The a_0 term has been neglected here, as much smaller than d. The t_0 and t_1 terms are easily obtained by the definite integrals:

$$t_0 = \frac{1}{T}\int_0^T \frac{dt}{d + a_1\cos(\omega_m t)} = \frac{1}{\sqrt{d^2 - a_1^2}}, \tag{15}$$

$$t_1 = \frac{2}{T}\int_0^T \frac{\cos(\omega_m t)dt}{d + a_1\cos(\omega_m t)} = -\frac{2}{a_1}\left(\frac{d}{\sqrt{d^2 - a_1^2}} - 1\right). \tag{16}$$

Reporting these expressions in Eq. (6) gives

$$\begin{aligned}(1-u^2)a_1\cos(\omega_m t + \varphi) - \frac{u}{Q}a_1\sin(\omega_m t + \varphi) + a_0 \\ = \frac{1}{Q}\sin\left(\omega_m t + \frac{\pi}{2}\right) - \frac{\pi\varepsilon_0 RV^2}{kZ^2}[t_0 + t_1\cos(\omega_m t + \varphi)] \\ - \frac{\alpha V^2}{kZ}\end{aligned} \tag{17}$$

from which can be deduced the constant term

$$a_0 = -\frac{\pi\varepsilon_0 RV^2}{kZ^2}t_0 - \frac{\alpha V^2}{kZ} \tag{18}$$

and a sinusoidal term as in the preceding section:

$$\left(1 - u^2 + \frac{iu}{Q}\right)\tilde{a}_1 = \frac{i}{Q} - \frac{\pi\varepsilon_0 RV^2}{Z^2}t_1\frac{\tilde{a}_1}{a_1}. \tag{19}$$

Introducing an effective gradient

$$g' = -\frac{\pi\varepsilon_0 RV^2 k t_1}{Z^2 a_1} = \frac{\pi\varepsilon_0 RV^2}{Z^2}\frac{2}{a_1^2}\left(\frac{d}{\sqrt{d^2 - a_1^2}} - 1\right) \tag{20}$$

one obtains expressions for the amplitude and phase:

$$a_1 = \frac{1}{\sqrt{u^2 + Q^2(1 - u^2 - g'/k)^2}} \tag{21}$$

and

$$\varphi = \arctan\left[\frac{Q(1 - u^2 - g'/k)}{u}\right]. \tag{21'}$$

The amplitude and the phase are still connected by the relation

$$\cos(\varphi) = ua_1. \tag{22}$$

Finally, the approximation presented above appears very similar to the linear approximation, the only difference consisting in different expressions for the gradient g [Eq. (10) or (20)]. Equation (20) tends towards Eq. (10) when a is much smaller than d, as can be verified in the following series:

$$\begin{aligned}g' &= \frac{\pi\varepsilon_0 RV^2}{Z^2}\frac{2}{a_1^2}\left(\frac{d}{\sqrt{d^2 - a_1^2}} - 1\right) \\ &= \frac{\pi\varepsilon_0 RV^2}{Z^2 d^2}\left(1 + \frac{3}{4}\frac{a_1^2}{d^2} + \frac{5}{8}\frac{a_1^4}{d^4} + \cdots\right).\end{aligned} \tag{23}$$

The above series shows that the linear approximation can be used up to $a = d/3$, with an error less than 10% on the gradient.

As g' depends on a_1, the function $a_1(d)$ cannot be extracted explicitly, as in Eq. (12). By reporting (20) in (19) and performing simple algebra, we obtain

$$\begin{aligned}\frac{a_1 Q g'}{k} &= \frac{2\pi\varepsilon_0 QRV^2}{kZ^2 a_1}\left(\frac{d}{\sqrt{d^2 - a_1^2}} - 1\right) \\ &= a_1 Q(1 - u^2) \pm \sqrt{1 - a_1^2 u^2},\end{aligned} \tag{24}$$

from where d can be extracted versus a_1:

$$d = a_1\frac{p+1}{\sqrt{p(p+2)}}$$

with

$$p = \frac{kZ^2 a_1}{2\pi\varepsilon_0 QRV^2}[a_1 Q(1 - u^2) \pm \sqrt{1 - a_1^2 u^2}]. \tag{25}$$

This expression describes completely the vibration of the system, and is studied in detail in the next section.

Some authors used the principle of least action and the Lagrangian of the system, to derive the oscillation equation in the case of Van der Waals force.[16,17] We verified that this method is also convenient for an electrostatic field of force, and gives exactly the same integrals and the same final expression (24) (see details in the Appendix). This seems natural, as the two methods are based on the same hypothesis, namely the sinusoidal nature of the oscillation and the neglecting of static flexure a_0 in Eq. (14).

Evidently the above methods are only approximations of the true oscillation, because they neglected the second order terms t_2 in the Fourier development.

When a_1 approaches d, i.e., when the tip comes very close to the sample, terms in $2\omega_m t$, $3\omega_m t$,… can no longer be neglected in Eq. (14) and the calculus becomes less precise.

C. Exact result and discussion

The exact solution of the dynamic equation (6) can be computed by a fourth order Runge-Kutta procedure, without

any of the simplification introduced above (i.e., without neglecting the static flexure a_0, and the higher order terms t_2, t_3,… in the Fourier series). At the initial time ($t=0$) the mass is released at the distance d, and then the oscillations are progressively established, up to a state of equilibrium. When the permanent regime is reached, the mean flexure a_0 and the amplitudes a_1, a_2 of the harmonics and the phases are computed, by a Fourier development of the $a(t)$ values over one period.

Whereas Q oscillations are considered by some authors[29] as sufficient to obtain the permanent regime, we have preferred to wait $5Q$ oscillations in order to obtain the final amplitudes more accurately.

The oscillation amplitude is reported in Fig. 1 in function of the distance d, for the two approximate models (linear as dots, nonlinear as continuous lines). The exact curves obtained numerically are superimposed over the nonlinear curve to 10^{-3}, for all cases studied, and cannot be separated from the nonlinear approximation at the scale of the figure. Only at very small distances ($d<0.01$), does a sudden jump-in appear in the exact curve, not present in the analytical curves, because of the neglected static flexure a_0.

The differences between linear and nonlinear curves are very simple to understand. The linear approximation gives too large amplitudes, even larger than the distance in the case $u=0.99$, which is absurd in noncontact mode. The nonlinear approximation seems to bend the curves in order to maintain $a<d$. The two models tend toward a common curve at large distances; they are pretty close together for $d>2$.

The curves in Fig. 1 have been calculated for a voltage of 1 V or 4 V, and for $R=20$ nm, which corresponds to a classic commercial tip radius. These parameters have been chosen to display in Fig. 1 typical behaviors of the system. Varying the other parameters as R, Z, Q or k will produce similar curves, because Eq. (25) depends only on the combined quantity $(kZ^2)/(QRV^2)$.

When the distance increases, all curves tend toward a constant, which is the free vibration amplitude of the system,

$$a_{\mathrm{inf}} = \frac{1}{\sqrt{u^2 + Q^2(1-u^2)^2}}, \tag{26}$$

amplitude at infinite distance. At finite distances, there are two different behaviors depending on the reduced frequency value u.

Case $u \geqslant 1$ (or $\omega_m \geqslant \omega_0$). As p should be positive in the radical of expression (25), and as $(1-u^2)$ is negative or null, then only the sign—can be chosen. There is only one curve $a(d)$.

Case $u<1$ (or $\omega_m < \omega_0$). As $(1-u^2)$ is now positive, then the sign + or − can be chosen in expression (25). There are two "d" solutions for an amplitude value greater than a_{inf}.

As mentioned in Ref. 19, some parts of these curves correspond to regimes not dynamically stable, namely when the $a(d)$ curves go backwards. On the other hand, when the microscope feedback is used to maintain a constant amplitude, only the part of the amplitude curve with a positive slope corresponds to a stable regulation.

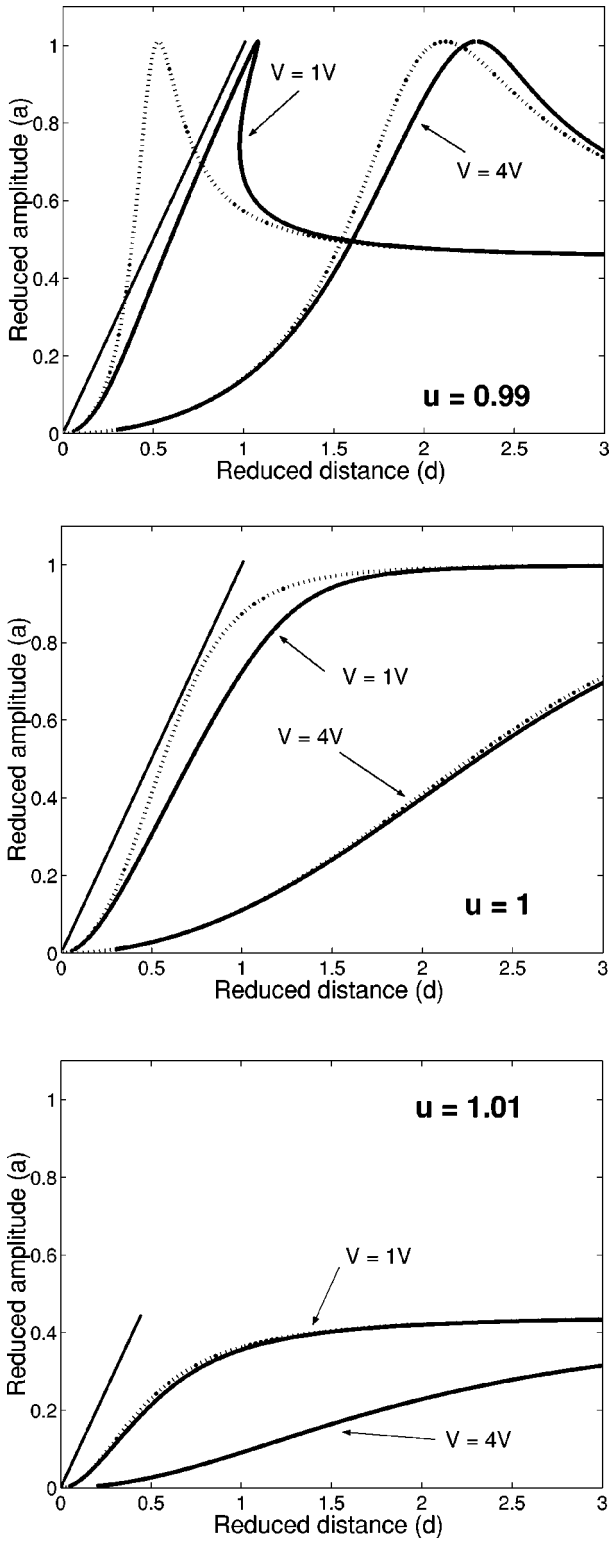

FIG. 1. Amplitude of vibration in function of the distance, for two voltage values $V=$ 1V and $V=$ 4V, for three frequency values ($u=f/f_0$). The solid curve is the exact value according to expression (21); the dotted curve is the linear approximation [expression (12)]. The numeric Runge Kutta values are superposed on the nonlinear curves. The thin straight line indicates the $a=d$ limit. The constants for the cantilever are $k=$ 1N/m, $Q=100$, apex radius $R=20$ nm, and free amplitude $Z_{\mathrm{max}}=10$ nm.

When two possible distances correspond to the same amplitude value, the lower value gives the closest tip sample distance, and the best sensitivity and resolution. This case corresponds to the sign + in Eq. (25).

The calculated phases are represented in Fig. 2; the nonlinear model and the exact solution appear identical. For $V=0$, the phase tends to values given by Eq. (22), which are $\phi=0$ for $u=1$ and $\pm 63°$ for the two other cases. As for the amplitude, some parts of the phase curves are not stable, for example the part of the curve where the phase decreases with distance, in the $u=0.99$ case, is not stable.

The results in Fig. 2 are presented for regularly spaced voltages, which allow us to appreciate the effect of the potential variations. The phase varies more rapidly in the region close to the angle of the curve, as will be developed in the next section.

The theoretical results obtained in Figs. 1 and 2 are compared to experimental results in Fig. 3 obtained with a classic silicon tip (Micromasch Ultrasharp NSC11, covered with conducting W_2C). The parameters of the cantilever (free frequency $f=59.9$ kHz, $Q=107$, $k=4.8$ N/m) have been independently measured. The experimental radius $R=35$ nm is deduced from the fit.

In order to present the curves with correct distance and amplitude values, the experimental points are recorded with a sinusoidal low frequency (2 Hz) applied voltage. The simultaneous fit of the envelope of the curve with the theoretical curves $V=0$ V and $V=3$ V, permits a correct evaluation of the free amplitude and of the distance origin. The potential V is here corrected from the contact potential difference, by applying an opposite constant potential, as in the Kelvin probe method. The efficiency of the correction can be observed in Fig. 3 as the successive phase minimums (corresponding alternatively to +3 V and −3 V) are both tangent to the fitted envelope.

Three important points are discussed below.

(1) We observed that the phase and the amplitude curves could not generally be fitted exactly. Most experiments on various *new tips* show amplitude and phase increasing towards the free limit more slowly than expected (in H^{-2} for the phase), in the 20–100 nm range. The effect of Van der Waals forces is negligible in the distance range, and would produce an opposite effect (phase decreasing in H^{-3} for a sphere). A force acting at longer distance is needed, and the expression for a cone seems to fit the curves better. After *several contacts* with the sample, the radius of the apex increases, in the 50 nm range, and the results are better fitted by a flat tip apex. In sum, experimental curves with the three following expressions have been observed.

For a cone (angle θ)

$$F_{cone} = -\frac{\pi\varepsilon_0 V^2 \ln\left(\frac{L}{H}\right)}{\ln^2\left(\tan\left(\frac{\vartheta}{2}\right)\right)}$$

and

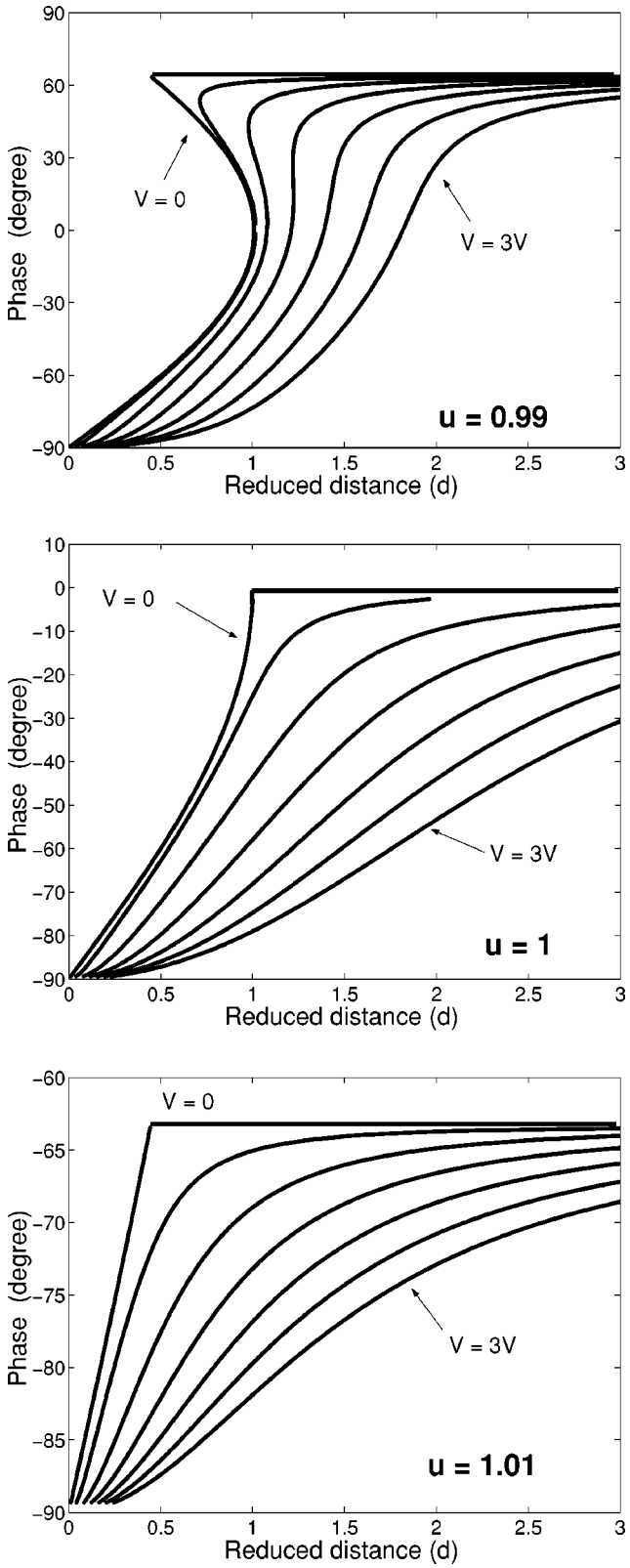

FIG. 2. Phase of vibration in function of the distance, for the voltage values $V=0$, 0.5, 1, 1.5, 2, 2.5, and 3 V, for the three frequency values (u). The curves are calculated in the non-linear approximation. The constants for the cantilever are the same as in Fig. 1.

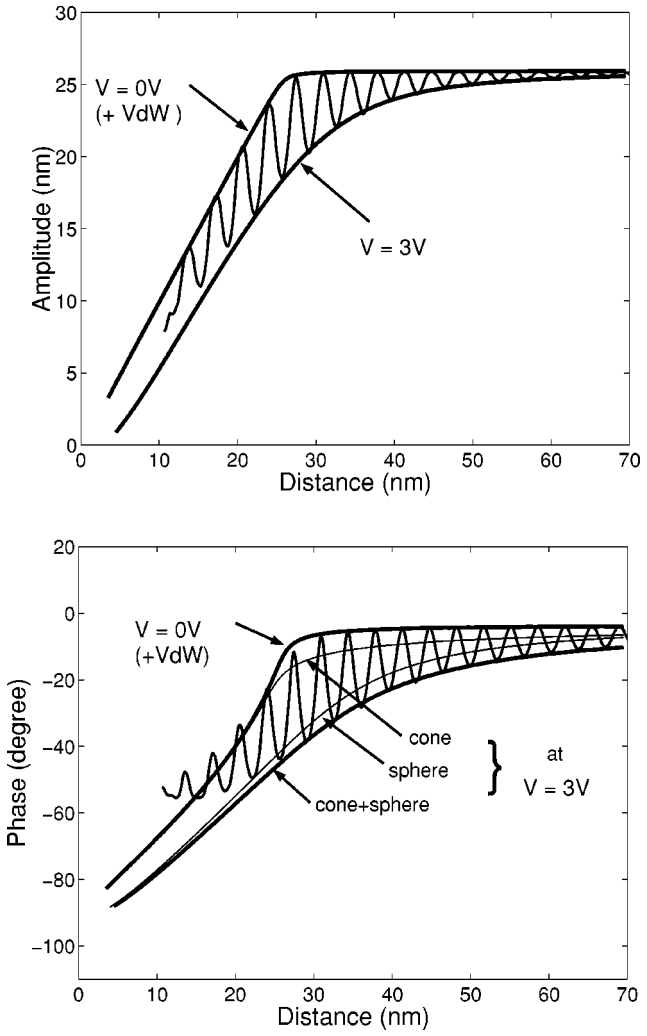

FIG. 3. Experimental amplitude and phase in function of distance, when a sinusoidal voltage is applied to the sample (the voltage amplitude is 3 V and frequency 2 Hz). The lower envelope is the theoretical values obtained for a *cone+sphere* shaped tip with a 20° aperture angle, a $R=35$ nm apex radius and for a 3 V voltage. The contributions of the sphere alone and of the cone alone are reported as thin lines. In the case $V=0$ V, a small amount of Van der Waals force has been added to stabilize the noncontact mode.

$$g_{cone} = \frac{\pi\varepsilon_0 V^2}{H \ln^2\left(\tan\left(\frac{\vartheta}{2}\right)\right)}. \tag{27}$$

For a sphere (radius R)

$$F_{sphere} = -\pi\varepsilon_0 V^2 \left(\frac{R}{H}\right)$$

and

$$g_{sphere} = \frac{\pi\varepsilon_0 V^2 R}{H^2}. \tag{28}$$

For a flat surface (radius r)

$$F_{flat} = -\frac{\pi\varepsilon_0 V^2}{2}\left(\frac{r}{H}\right)^2$$

and

$$g_{flat} = \frac{\pi\varepsilon_0 V^2 r^2}{H^3}. \tag{29}$$

For an intermediary shape (in the Fig. 3 for example), the fit was obtained by the sum of two force expressions ($F_{\text{cone}}+F_{\text{sphere}}$), indicative of a cone with a spherical apex. The F_{cone} and the F_{sphere} contributions are represented separately in the phase curves. In the 20–50 nm range, the sphere term is predominant, the two terms are equal at 80 nm, and the cone term became more important at a larger distance. We are aware that if nearly all the experimental curves can be fitted by a sum of the above expressions,[30,31] it does not mean that the exact shape of the tip apex is determined. In particular the expression for a true cone with a spherical apex is more complicated than the above sum (see Hudlet[28] for an analytical expression or Belaidi[27] for a numerical simulation).

Finally, it should be considered that the exact shape of the tip apex is not important in itself, as only the $F(d)$ curve determines the oscillation behavior, the sensitivity and the resolution discussed here. Experimentally, the slope of the phase curve $\varphi(d)$ or of the gradient curve $g(d)$ in log-log plot is indicative of the major electrostatic contribution (slope −3 for a flat, −2 to a sphere, −1 for a cone). The flat tip slope (−3) is similar to the slope for the Van der Waals force acting on a sphere, and produces the same dynamics. The middle case (slope −2 for an electrostatic force in the sphere-plane geometry) is the only case analyzed in the following sections.

(2) Another difficulty in fitting the experimental curves in Fig. 3, comes from the $V=0$ curve. With a sinusoidal applied voltage (amplitude 3 V), we are sure that the voltage difference between the tip and the sample passes regularly by zero, whatever the eventual contact potential difference between the two materials. Then, the upper envelope of the experimental curve should correspond to the $V=0$ (no force) theoretical solution: the amplitude is constant at a large distance ($H>30$ nm), and limited by the $d=a$ line at distances below the free amplitude ($H<26$ nm). This simple shape (two straight lines) is not observed in Fig. 3, probably due to the Van der Waals forces or residual charges,[30] neglected in the model, and preponderant when the main electrostatic forces disappear (for $V=0$). In order to fit better the experimental curve in Fig. 3, a small amount of Van der Waals force has then been added to the theoretical values.

(3) The above calculations in noncontact mode do not include the dissipation process, which arises when the tip approaches the surface. The dissipation induces a phase shift, as discussed in Refs. 32–34. The onset of such an effect can be clearly seen in Fig. 3, where the experimental phase is higher than calculated at small distances. The same effect is clearly observed at low amplitude in Ref. 33. We have not attempted to fit this part of the curve, as the dissipation processes are out of the scope of the present article.

III. SENSITIVITY

The sensitivity is defined as the ability of the system to differentiate two close values for the voltage V. We introduce the following definition:

$$\text{Phase sensivity} = -\frac{d\varphi}{dV} \quad \text{or} \quad \text{Amplitude sensivity} = -\frac{da_1}{dV} \tag{30}$$

the sign-being used to obtain positive values in most cases (notably for $u>1$).

Expression for the sensitivity can be deduced easily from expression (24), written as

$$\frac{CV^2}{a_1}\left(\frac{d}{\sqrt{d^2-a_1^2}}-1\right) = a_1 Q(1-u^2) \pm \sqrt{1-a_1^2u^2}$$

with

$$C = \frac{2\pi\varepsilon_0 QR}{kZ^2}. \tag{31}$$

One obtains

$$\frac{da_1}{dV} = \frac{2CV\left(\frac{d}{\sqrt{d^2-a_1^2}}-1\right)}{\frac{a_1 dCV^2}{(d^2-a_1^2)^{3/2}} - 2a_1Q(1-u^2) \mp \sqrt{1-a_1^2u^2} \pm \frac{a_1^2u^2}{\sqrt{1-a_1^2u^2}}}. \tag{32}$$

The amplitude and the phase being related according to expression (22), the amplitude and the phase sensitivity are related by

$$\frac{da_1}{dV} = \frac{da_1}{d\varphi}\frac{d\varphi}{dV} = -\frac{\sin\varphi}{u}\frac{d\varphi}{dV} \tag{33}$$

Then

$$\frac{d\varphi}{dV} = \frac{-u}{\sqrt{1-u^2a_1^2}}\frac{da_1}{d\varphi}. \tag{34}$$

In Fig. 4 the phase sensitivity is reported, calculated theoretically from the expressions (32) and (34).

In the case $u \geqslant 1$, the sensitivity is always positive and presents a maximum, whose position and value depends on the reduced frequency "u," and on the combined RV^2 term. For low voltage (or radius), the values of maximum sensitivity lie in the $0<d<1$ distance range, indicating that working in the non-linear domain is essential for a good sensitivity

For $u<1$, positive and negative sensitivities are obtained. The sensitivity reaches a very high value, for certain distances. This induces several problems in experiments, as the electrical contrast becomes very sensitive to the distance, and may reverse in certain conditions.

IV. STABILITY

The vibration modes found theoretically by the resolution of the differential equation (6) are not necessarily stable. This instability has two main reasons.

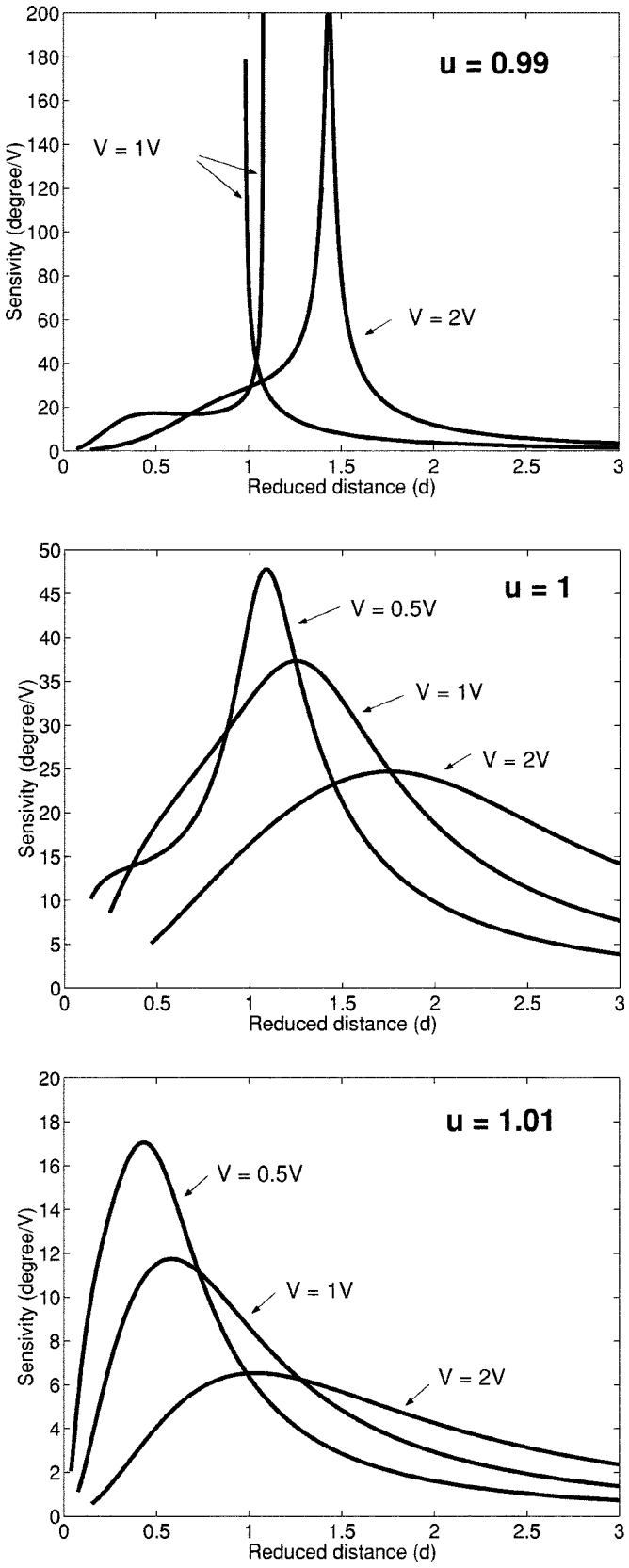

FIG. 4. Sensitivity of the microscope to voltage variations, sensitivity$=-d\varphi/dV$. The constants for the cantilever are $k=1$ N/m, $Q=100$, tip apex radius $R=20$ nm, and free amplitude $Z=10$ nm.

First, some solutions correspond to theoretically unstable movement.[15,17] Any disturbance, no matter how small, induces a diverging process, which after a short time converges toward a different vibration state. This is the case of the backward part of the superior $a(d)$ curves in Fig. 1.

The second reason occurs in experiments, when several stable vibrations are possible at one distance. For example, when $d<1$ the noncontact vibration mode and the tapping vibration mode are both stable,[35–38] they correspond to attractive or repulsive regimes. Three stable states may then exit in the case of soft samples.[39]

Small experimental disturbances (such as thermal noise, sample roughness or a small shock on the system) may induce the transit from one mode to the other.[40,41] If this transit is easier in one sense than in the other, then a mode appears more stable than the other. Experimentally the system adopts the most stable mode, even if another is possible theoretically.

Examples of such behavior are presented in Fig. 5, where the oscillating amplitude is presented during the transient phase. For a purely sinusoidal vibration, the position and velocity at the time $t=0$ are

$$Z_0 = [\mathrm{Re}(\tilde{A}e^{i\omega t})]_{t=0} = \mathrm{Re}(\tilde{A}) \text{ and } V_0 = \left[\frac{d}{dt}\mathrm{Re}(\tilde{A}e^{i\omega t})\right]_{t=0}$$

$$= \omega\,\mathrm{Im}(\tilde{A}).$$

Our representation is then similar to the Poincaré plot used in Refs. 40 and 41 and enables us to define the basins of attraction of the different modes. Starting from an initial condition (dots at the beginning of the curves), the amplitude and phase evolve towards a permanent vibration [noncontact or tapping in the Fig. 5(a)]. The complex plane can be divided into zones where the oscillation evolves towards one or the other stable mode. In Fig. 5(a), all initial oscillations below the dotted line converge towards the noncontact mode and all initial oscillations above the dotted line converge towards the tapping mode. The basins of attraction are of similar size. As only initial points inside the noncontact circle have been tested, the spiral structure of Refs. 40 and 41 is not apparent.

In Fig. 5(b), the case of 3 stable modes on a stiff sample is represented. The basin of attraction for the low amplitude noncontact mode (nc1) is much larger than the basin for the high amplitude noncontact mode (nc2). At this frequency, the basin for the tapping mode is so reduced that it cannot be plotted clearly at the scale of the figure. For these experimental conditions, the tapping mode is absolutely stable but very sensitive to any disturbance.

All the above modes are totally stable at the end of the transient time, but can commute from one to the other if a disturbance occurs. In order to quantify the relative stability of any mode, we introduce a measure of the stability, defined as the amount of disturbance needed to pass from one mode to another. As the disturbance is generally a casual variation of distance d, the maximum disturbance Δd can be calculated numerically by applying a sudden jump of Δd and observing if the system returns to the initial mode or changes toward another state. In Fig. 5, the stability can be measured as the horizontal jump needed to translate the mode from a stable point toward another basin of attraction.

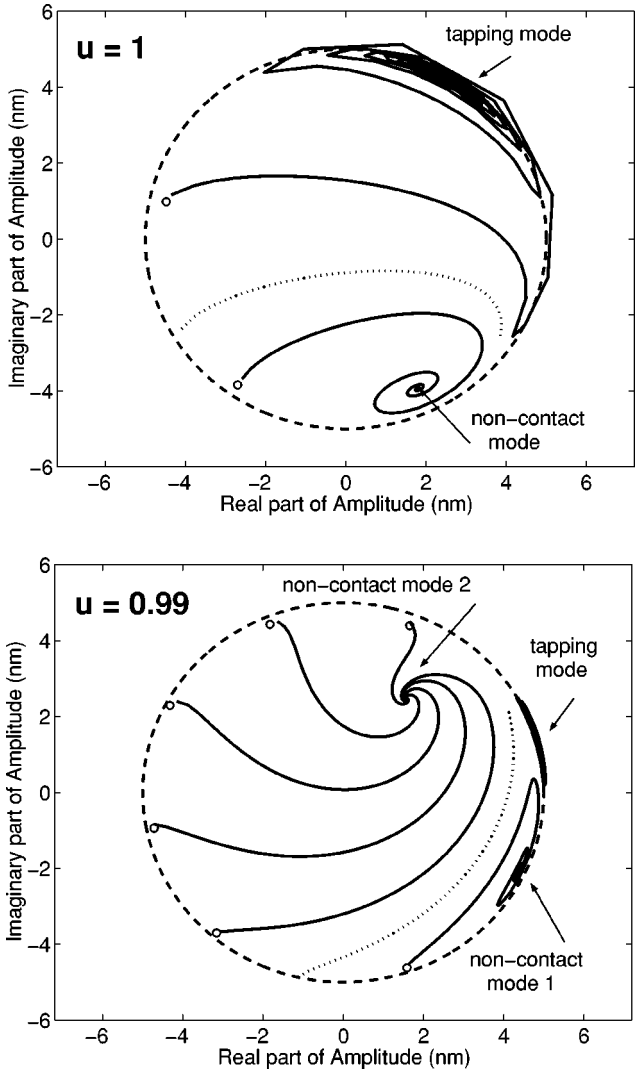

FIG. 5. Evolution of the oscillating amplitude (real and imaginary part) during the transitory phase. The dashed circle indicates the contact $d=a$ condition. Points inside the circle correspond to noncontact oscillations, whereas points outside the circle correspond to intermittent contact oscillations. Depending on the initial conditions (dots), the oscillation tends towards different modes. All initial conditions within the circle have been tested numerically in order to define attraction zones. The limit between the zones is noted as the dotted line. The common experimental conditions are distance $H=5$ nm, voltage $V=0.5$ V, tip radius $R=20$ nm, and reduced elastic modulus of tip and sample $E^*=66$ GPa. Upper diagram: reduced frequency $u=1$. Two zones appear: one that leads to the tapping mode and the other to the noncontact mode. Free amplitude $Z=10$ nm; reduced distance $d=H/Z=0.5$. Lower diagram: reduced frequency $u=0.99$. The experiment conditions have been chosen to produce the rare case where three stable modes coexist (2 noncontact modes and the tapping mode). Free amplitude $Z=5.5$ nm; reduced distance $d=H/Z=0.91$.

The main results can be observed in Fig. 6. The vertical scale represents the magnitude Δd of the stability.

For $u=1$ there are only 2 stable movements, the noncontact and the tapping mode.

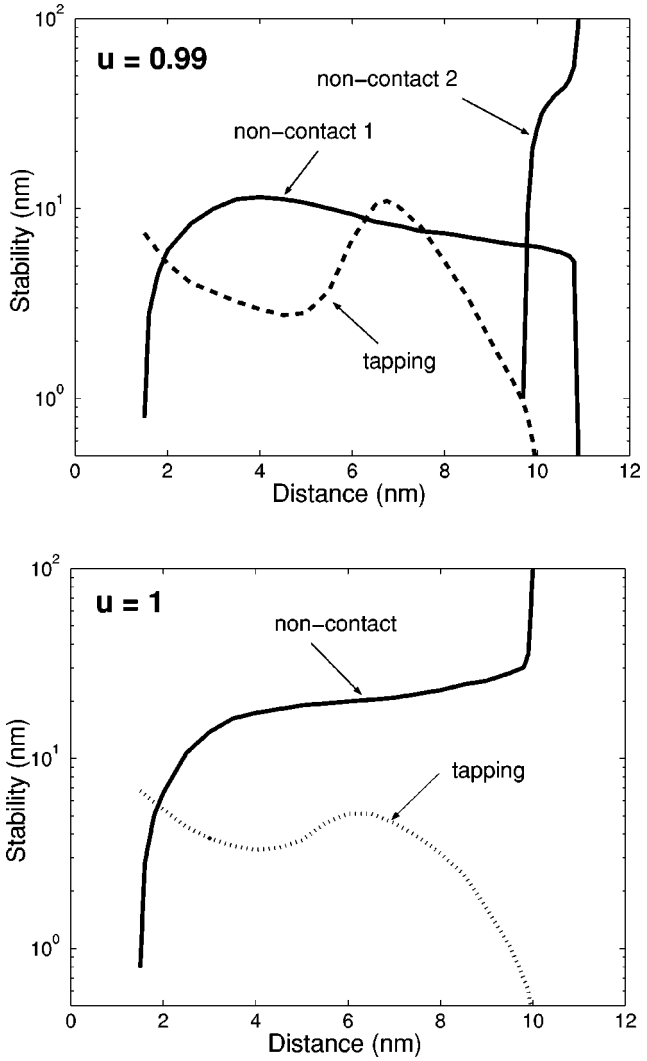

FIG. 6. Stability of the mode of oscillation of the cantilever for two values of the frequency ($u=0.99$ and 1.00). The oscillating conditions are free amplitude $Z=10$ nm, apex radius $R=20$ nm, and voltage $V=1$ V. The case $u=1.01$ shows unconditional noncontact stability and cannot be represented.

For $u<1$ there are 2 or 3 stable movements, depending on the d values, one tapping mode and 1 or 2 noncontact modes, as already apparent in Fig. 1. The stability of the tapping mode decreases as the distance approaches the free amplitude ($d\sim 1$). When d increases slightly above 1, the only stable mode remaining is the noncontact mode.

For $u>1$ the noncontact mode is unconditionally stable.

An important result not mentioned in the above references is the possible existence of 2 stable noncontact modes with a purely attractive force (Figs. 5 and 6), due to the nonlinearity of the force. Adding a repulsive force term leads to a third stable mode, the tapping mode. We note in Fig. 6, that for most distances d, only two stable modes are present, tapping and noncontact 1 for $d<1$, or noncontact 1 and noncontact 2 for $d\sim 1$. Only in a very small distance interval, slightly lower than 1, does the possibility of three stable modes appear [as in Fig. 5(b)]. These three stable modes could produce, in experimental amplitude-distance curves, a double jump, not already mentioned in the literature, probably because of the very small basin of attraction of the third mode, which is simply missed.

For a free amplitude of 10 nm, a sudden topographic jump in the order of 1 nm is sufficient to induce a mode commutations, from noncontact mode to tapping mode and vice versa. These sudden jumps should be avoided during the scans, so a very stable mode is recommended. For instance, in the conditions of Fig. 6, the recommended working distance is $H>10$ nm (equivalent to $d>1$), to obtain stable scans.

It is difficult to deduce general rules on the stability of the different modes, except the following quasievident conclusions.

The noncontact mode is very stable if the amplitude is much smaller than the distance.

Large voltage (or radius) enhances the stability of the noncontact mode.

Null voltage leads to the tapping mode, because the Van der Waals attractive force is too weak to stabilize the noncontact mode.

Experimentally, it is recommend to choose $u\geqslant 1$ and a distance around $d=1$, to be at the lowest distance with unconditional noncontact stability.

V. LATERAL RESOLUTION

Lateral resolution is the ability of the system to observe the surface potential of small objects with acuity. Several practical definitions for the resolution can be found, according to the type of object to be imaged.[42,43] In microelectronic applications, objects are often bidimensional, with linear edges, such as tracks, or flat layers in transversally cut components. For this reason we introduce, as a standard sample, the line of separation of two potentials (V_1 and V_2) on a flat surface, as represented in Fig. 7.

Varying the position X of the tip gives a phase that passes continuously from the values φ_1 to φ_2. We defined the resolution as the distance ΔX for which the signal varies from the ratio $\frac{1}{4}$ to $\frac{3}{4}$ of the maximal variation ($\varphi_2-\varphi_1$), as represented in Fig. 7(b) (noted Δ_{L50} in Ref. 41).

Calculating the resolution needs an expression for the electrostatic force derived below. In the limit case where the tip-sample distance H is much smaller than the tip radius R, the electric field between the tip and the sample can be taken as vertical, and the force obtained by simple integration of the electrostatic pressure

$$P(x,y)=\frac{\varepsilon_0}{2}\frac{V^2}{z^2}=\frac{\varepsilon_0}{2}\frac{V^2}{\left(H+\dfrac{x^2+y^2}{2R}\right)^2}, \tag{35}$$

over the sample plane, which has a potential V_1 for $x<X$ and V_2 for $x>X$. The force is expressed as

$$\begin{aligned}|F_z| &= \int_{-\infty}^{+\infty} dy \int_{-\infty}^{X} P_1(x,y)dx + \int_{-\infty}^{+\infty} dy \int_{X}^{+\infty} P_2(x,y)dx \\ &= \frac{\pi\varepsilon_0 R}{2H}\left(1+\frac{X}{\sqrt{X^2+2RH}}\right)V_1^2 \\ &\quad + \frac{\pi\varepsilon_0 R}{2H}\left(1-\frac{X}{\sqrt{X^2+2RH}}\right)V_2^2\end{aligned}$$

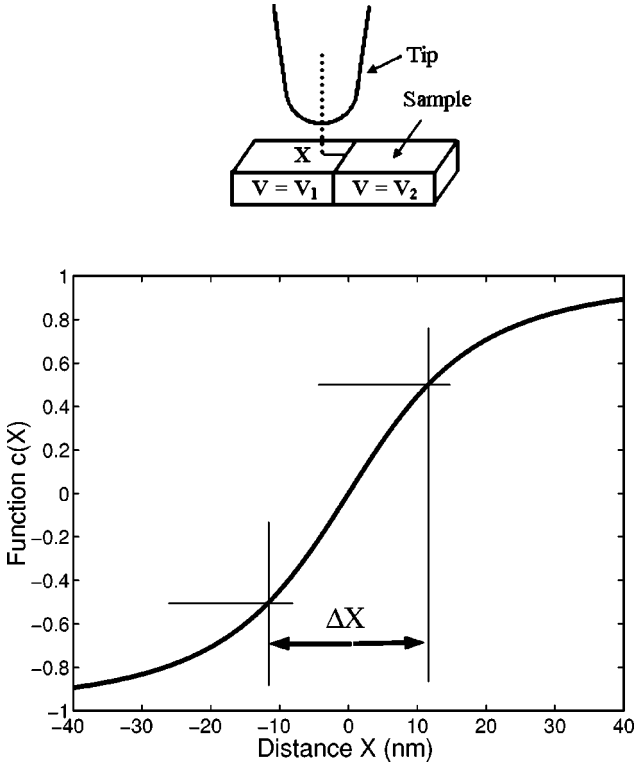

FIG. 7. (a) Scheme of the tip and sample relative position, which indicates the distance X between the tip axis and the potential step. (b) Function $c(X)$ for $R=20$ nm and $H=10$ nm. The resolution is here $\Delta X=23$ nm.

$$= \frac{\pi\varepsilon_0 R}{4H}(V_1^2+V_2^2) + \frac{\pi\varepsilon_0 R}{2H}\frac{X}{\sqrt{X^2+2RH}}(V_1^2-V_2^2). \quad (36)$$

The gradient can be obtained by deriving the above expression, $G=dF/dH$:

$$G_z = \frac{\pi\varepsilon_0 R}{4H^2}(V_1^2+V_2^2) + \frac{\pi\varepsilon_0 R}{2H^2}\frac{X(X^2+3RH)}{(X^2+2RH)^{3/2}}(V_1^2-V_2^2). \quad (37)$$

According to expression (12), the phase follows the variation of the gradient, and presents then the behavior reported in Fig. 7(b).

A. Linear approximation

The phase passes continuously from φ_1 when the tip is over the V_1 potential to φ_2 when the tip is over the V_2 potential. The function $c(X)=X(X^2+3RH)/(X^2+2RH)^{3/2}$ is characteristic of the phase variation when the tip passes above the limit of the two bands. This function varies between -1 and $+1$.

Using the above definition for the lateral resolution (ΔX is the distance between the points where the function $c(X)$ is $-1/2$ and $+1/2$), we obtain the resolution in measures sensitive to the gradient:

$$\Delta X = 1.047\sqrt{RH}. \quad (38)$$

Similar results in the form of a constant multiplied to $\sqrt{RH}$ can be obtained, with an adapted expression of the force, in the case of different objects, as individual charge or vertical dipole.

The expression (38) is somewhat different from Ref. 43 because of the different assumptions in the electric field. McMurray and Williams consider the tip as a point charge; its model applies then to a large tip-sample separation ($H>R$), whereas we consider the tip as a sphere very close to the sample, giving here the low distance approximation ($H<R$).

B. Nonlinear approximation and exact solution

In the nonlinear regime, the calculus of the resolution is less simple, because the effective gradient [expression (20)] depends on the distance and on the vibration amplitude. The exact resolution can however be evaluated by solving numerically the vibration equation by the Runge Kutta procedure, including the exact force (36), in order to obtain the $c(X)$ curve.

Using the same definition of lateral resolution (interval ΔX which corresponds to $1/4$ to $3/4$ ratio of the maximum variation of the phase), the resulting resolution of the system is determined, and represented in Fig. 8 as dots. The following results can be derived.

For $u \geqslant 1$, the resolution is an increasing function of distance, indicating that the best distance for obtaining sharp images is the smallest one.

For $u<1$, the resolution shows a plateau in the distance range (0–1), which is related to the fact that the $a(d)$ curve (Fig. 1) is nearly parallel to the $d=a$ line. In this range, the minimum distance $(d-a_1)$ is relatively constant.

An approximation corresponding to the nonlinear model can now be derived. As the electrostatic interaction has its maximum effect when the tip is close to the sample plane, the true resolution should be better than $1.047\sqrt{RH}$, which is calculated for the mean distance H.

A better approximation is obtained as follows: first, we introduce an effective distance d_{eff}, which is the distance where the electrostatic force is equal to the mean force, averaged over a period. According to expression (15), the effective distance is given by

$$d_{eff} = \sqrt{d^2 - a_1^2} = \sqrt{d_{\min} d_{\max}}. \quad (39)$$

Secondly, this value is used instead of the mean distance d in Eq. (38). Expressing the equation in absolute units, we obtain

$$\Delta X = 1.047\sqrt{RH_{eff}} = 1.047\sqrt{RZd_{eff}} = 1.047\sqrt{R}\sqrt[4]{H_{\min}H_{\max}}. \quad (40)$$

This calculated resolution for the nonlinear approximation is reported in Fig. 8. As expected, this approximation is much better than the linear one, and sufficient for practical application.

According to the values in Fig. 8, the best resolution is obtained for the smallest distance. In some cases (here for

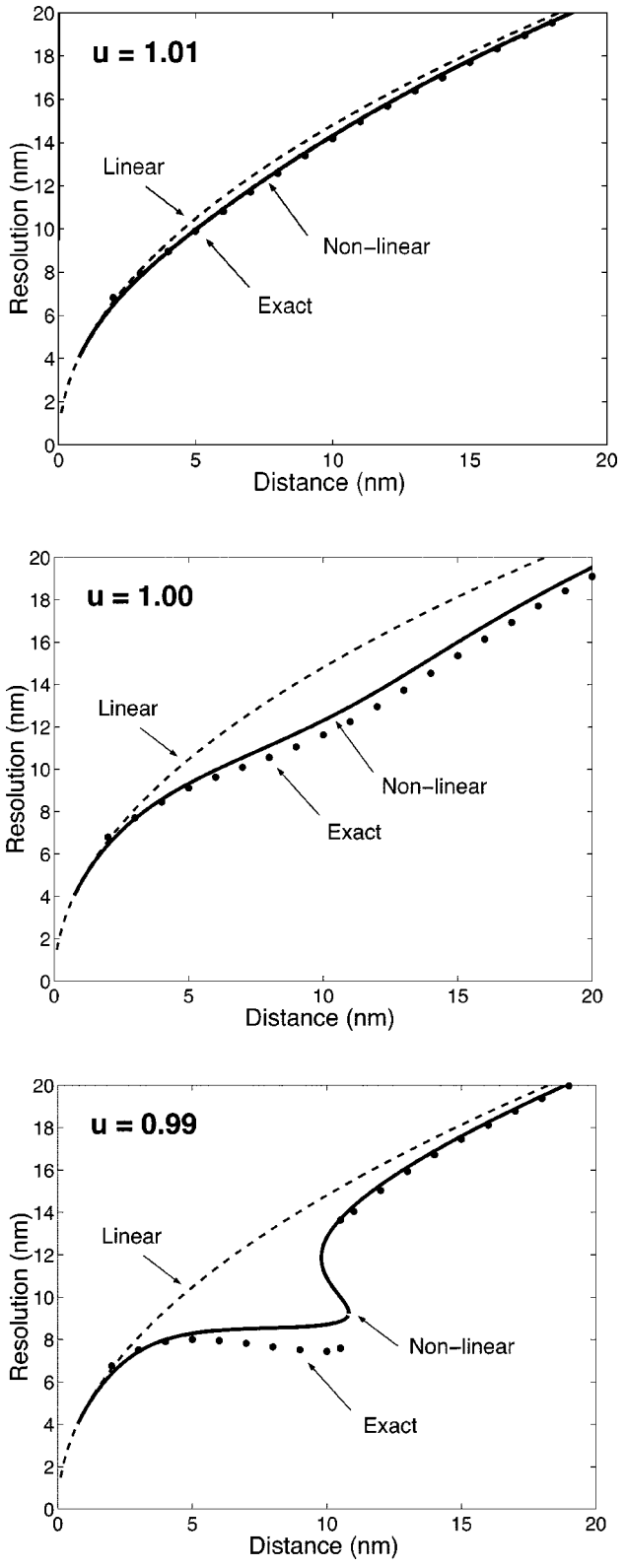

FIG. 8. Resolution of the microscope in function of the tip-sample mean distance for different reduced frequencies. The resolution is calculated according to then expression (38) (linear model), expression (40) (nonlinear model) and by the Runge Kutta procedure (exact). The oscillating conditions are free amplitude $Z=10$ nm, voltage=1 V, tip apex radius $R=20$ nm, quality factor $Q=100$, and cantilever stiffness $k=1$ N/m.

$u=0.99$), the resolution shows a plateau. This plateau probably corresponds to favorable experimental conditions, as the resolution is good, and nearly independent of distance.

We verify also that, in nonlinear mode, resolution can be much lower than the apex radius.

VI. STUDY OF A CURIOUS NONLINEAR CASE ($u=1$ AND $d=1$)

It appears above that the vibration with a working frequency equal to the natural frequency of the system ($u=1$), and with a distance equal to the free amplitude ($d=1$), is one of the best noncontact modes for scanning the voltage of a sample, combining high sensitivity to the voltage, high resolution and an absolute stability.

In this particular case, Eq. (24) becomes

$$\frac{2\pi\varepsilon_0 QRV^2}{kZ^2}\left(\frac{1}{\sqrt{1-a_1^2}}-1\right)=a_1\sqrt{1-a_1^2}, \tag{41}$$

which is a 5th degree equation in a_1, which can be simplified in some useful cases. As good spatial resolutions are obtained only for small radius R, we further suppose that the term $2\pi\varepsilon_0 QRV^2/kZ^2$ is much smaller than 1. As a result a_1 is close to 1, and Eq. (41) can be developed in series, and solved to the first order:

$$a_1=1-\frac{\pi\varepsilon_0 QRV^2}{kZ^2}. \tag{42}$$

The phase is then deduced from Eq. (22):

$$\varphi=-\arccos[ua_1]=-\sqrt{\frac{2\pi\varepsilon_0 QRV^2}{kZ^2}}=-\sqrt{\frac{2\pi\varepsilon_0 QR}{kZ^2}}|V|. \tag{43}$$

The minimum distance between the tip and sample is given by

$$H_{\min}=Z(1-a_1)=\frac{\pi\varepsilon_0 QRV^2}{kZ}. \tag{44}$$

The sensitivity is obtained by differentiating (43):

$$\text{Sens}=-\frac{d\varphi}{dV}=\sqrt{\frac{2\pi Q\varepsilon_0 R}{kZ^2}}. \tag{45}$$

The approximate lateral resolution is obtained by replacing (44) and $H_{\max}=2Z$ in (40):

$$\Delta X=1.047\left[\frac{2\pi\varepsilon_0 QR^3V^2}{k}\right]^{1/4}. \tag{46}$$

The accuracy of the above approximation can be verified in the Table I for $H=10$ nm, $V=0.2$ V, $R=20$ nm, $Q=100$, $k=3$ N/m, and $Z=10$ nm.

As expected for this distance, the linear model fails totally. The nonlinear model gives a satisfying approximation.

We consider this case as curious because of expression (43), in which the phase of the vibration depends on $|V|$, instead of V^2, as usual in the other cases. In Fig. 9, for

TABLE I. Comparison between linear and nonlinear approximations, for the case $u=1$ and $d=1$.

	Linear approximation	Nonlinear approximation	Exact values
a	9.9997 nm	9.926 nm	9.933 nm
φ	0.42°	6.98°	6.63°
$H_{\min}$	0.0003 nm	0.074 nm	0.067 nm
Sens	4.2°/V	34.9°/V	33.1°/V
ΔX	14.8 nm	4.3 nm	3.0 nm

example, one can verify the linear dependence $\varphi(V)$ for $d=1$ ($H=10$ nm). For a larger distance, $d=1.2$ ($H=12$ nm), the $\varphi(V)$ exhibits the more classic parabolic dependence.

For $d=1$, the voltage sensitivity is also constant [expression (43)], instead of decreasing with the voltage as in linear modes. This particularity would allow the detection of a much lower voltage than permitted in the other configurations, and finally constitutes the interest of the studied case.

VII. DISCUSSION AND CONCLUDING REMARKS

The noncontact mode at short distance, with electrostatic forces, appears relatively simple, with a general behavior similar to the more studied Van der Waals forces. We show that the development of the force in the Fourier series is sufficient, at the first order, to provide precise analytical approximation.

Moreover, this article combines several notions related to the experiments, such as sensitivity, stability and lateral resolution, in order to determine which the best experimental conditions are.

The free parameters in an experiment are the working frequency (or $u=\omega_m/\omega_0$), the maximal amplitude Z, the mean distance D (or $d=D/Z$), and the tip voltage V relative to the sample. From all the above expressions and figures it is clear that sensitivity, stability and lateral resolution cannot be optimal at the same time.

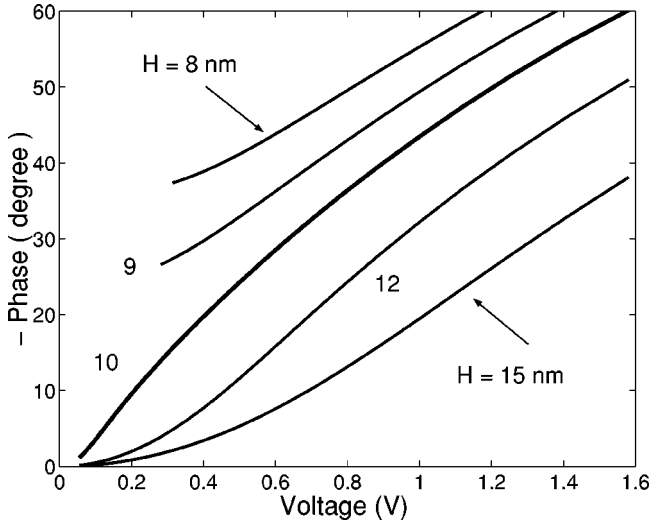

FIG. 9. Phase of the oscillation in function of the tip voltage, for several tip-sample mean distances H. The oscillating conditions are free amplitude $Z=10$ nm, reduced frequency $u=1$, and tip apex radius $R=20$ nm. The curves for $H=8$ nm and $H=9$ nm are not plotted for low voltages, because they are unstable.

(1) Stability. A small working distance seems to be favorable, both for sensitivity and for resolution, but its reduction below the free amplitude is limited by the stability of the noncontact vibration. As the stability of the noncontact mode is difficult to predict theoretically, we can understand the method often used by experimentalists, i.e., the tip distance is lowered until the system begins to be unstable, and then restabilized by a small distance increase. However, we show that working with frequency above the free frequency of the cantilever ($u>1$) gives the best stability conditions.

(2) Sensitivity. For a given tip, the sensitivity can be chosen as great as desired, because infinite sensitivity is theoretically predicted. The amplitude, distance and voltage conditions for infinite sensitivity can be found in Fig. 2; they coincide with points where the slope of the $\varphi(d)$ is vertical. Experimentally, the precise conditions for maximal sensitivity are difficult to find and maintain during the scans, because they are very sharp, as seen in the upper Fig. 4. It seems preferable to choose a lower sensitivity, with more flexible experimental conditions. As the sensitivity curve $S(d)$ decreases and flattens when the frequency and the voltage increase, reduced frequencies equal or greater than 1 are recommended. For example, $u=1$ and $V=1$ V (in the middle Fig. 4), give relatively good sensitivity in the range $1<d<1.5$. The special case treated in Sec. VI is therefore a good compromise.

(3) Lateral resolution. The theoretical resolution improves (decreases) when the tip sample distance decreases, and seems to vanish in all conditions for $d=0$. Experimentally, this is evidently not the case for two reasons. First we neglected the atomic nature of the tip and sample, and secondly we supposed that the tip sample distance can be as low as needed. In ambient air, for instance, the onset of a liquid meniscus between the tip and sample prevents us approaching the tip closer than some nanometers. In vacuum, when the tip-sample distance decreases, the Van der Waals force increases more rapidly than the electrostatic forces, and for small distances, may exceed them. In this case, the attractive force becomes independent of the voltage, and the voltage contrast gradually disappears. This induces also a minimum distance called $H_{\min}$. When this minimum distance is reported in expression (40) and $H_{\max}=2D-H_{\min}\cong 2D$, one obtains

$$\Delta X_{\text{limit}} = 1.047\sqrt[4]{2R^2DH_{\min}}, \tag{47}$$

which is the best lateral resolution realizable in an experiment at the mean distance D. If this limit resolution is compared, in Fig. 10, to the theoretical resolution deduced from the general expression (40), it appears that distance and voltage values cannot be selected freely. Resolutions lower than the limit are prohibited because the tip would pass too close from the sample. For instance, it is evident in Fig. 10 that the tip voltage should not be reduced below a certain value (0.5 V in the middle Fig. 10), in order to avoid such closeness.

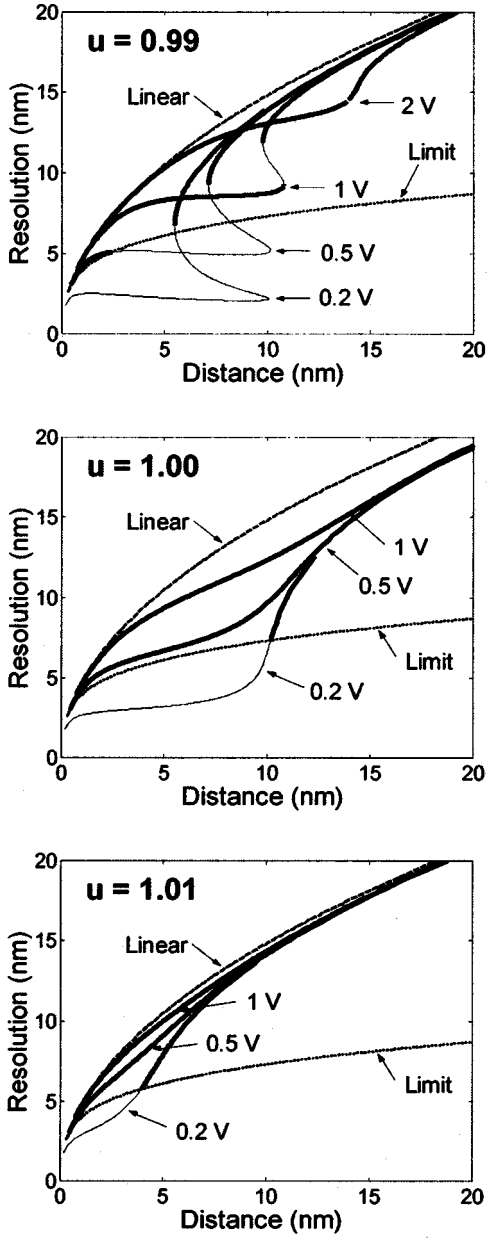

FIG. 10. Resolution of the microscope in function of the tip-sample mean distance, for different applied voltages and frequencies. The resolution is calculated according to expression (38) (linear model) and expression (40) (nonlinear model). The oscillating conditions are free amplitude $Z=10$ nm, voltage$=1$ V, tip apex radius $R=20$ nm, quality factor $Q=100$, and cantilever stiffness $k=1$ N/m. The minimum distance for the limit resolution is $H_{\min}=0.3$ nm.

Although there are no experimental conditions which give simultaneously the best sensitivity, stability and lateral resolution, the frequency $u=1$ seems nearly optimal in most cases. The distance around $d=1$ is favorable for the sensitivity, whereas lower values are recommended for the lateral resolution. Finally the tip-sample voltage should be notable, so that a too close approach between the tip and the sample is avoided. In vacuum, the ultimate resolution is determined by the ratio of Van der Waals to electrostatic forces, and is therefore closely related to the microscopic nature of the sample, i.e., the covalent or ionic character of the surface and tip atoms.

APPENDIX

We will demonstrate below that the variational method, applied on the sphere-plane electrostatic interaction, is absolutely similar to the Fourier method used above in the derivation of Eq. (24). We follow below the notation used by J.P. Aimé, in the Van der Waals case.[17]

The Lagrangian L is composed of three terms, representing the kinetic energy, the potential energy and the dissipation,

$$L(z,\dot{z},t) = T - U + W, \tag{A1}$$

$$L = \frac{1}{2}m\dot{z}^2 - \left[\frac{1}{2}kz^2 - zF_{exc} + E_{elec}\right] - cz\dot{z}, \tag{A2}$$

with the electrostatic potential energy, referred to the mean distance D:

$$E_{elec} = -\int_0^z \frac{\pi\varepsilon_0 RV^2}{D+z}dz = -\pi\varepsilon_0 RV^2 \ln\left(\frac{D+z}{D}\right). \tag{A3}$$

As the oscillation is supposed sinusoidal,

$$z(t) = A\cos(\omega_m t + \varphi), \tag{A4}$$

the action S is the integral of the Lagrangian over a period. The action is dissociated in three terms,

$$S = S_0 + S_{elec} + S_{diss}, \tag{A5}$$

where S_0, S_{elec}, and S_{diss} are, respectively, the action of the harmonic oscillator without dissipation, the action of the electrostatic force, and the action of the dissipating term. S_0 and S_{diss} are similar to the results in Ref. 17, except for $\sin(\varphi)$ which comes from our different drive reference:

$$S_0 = \frac{\pi m}{2\omega}A^2(\omega^2 - \omega_0^2) + \frac{\pi F}{\omega}A\sin(\varphi), \tag{A6}$$

$$S_{diss} = -\frac{\pi m\omega_0}{Q}A\underline{A}\sin(\varphi - \underline{\varphi}), \tag{A7}$$

$$S_{elec} = \int_0^{2\pi/\omega} E_{elec}dt. \tag{A8}$$

The S_{elec} term is not evaluated explicitly, only its derivatives are needed:

$$\frac{\partial S_{zelec}}{\partial A} = \frac{\partial}{\partial A}\int_0^{2\pi/\omega} E_{elec}dt = \int_0^{2\pi/\omega}\frac{\partial}{\partial A}E_{elec}dt$$
$$= \frac{2\pi^2\varepsilon_0 RV^2}{\omega A}\left(\frac{D}{\sqrt{D^2 - A^2}} - 1\right), \tag{A9}$$

$$\frac{\partial S_{zelec}}{\partial \varphi} = \frac{\partial}{\partial \varphi}\int_0^{2\pi/\omega} E_{elec}dt = \int_0^{2\pi/\omega} \frac{\partial}{\partial \varphi}E_{elec}dt = 0. \tag{A10}$$

The minimization of S with respect to A and φ gives

$$\frac{\partial S}{\partial A} = \frac{\pi m}{\omega}A(\omega^2 - \omega_0^2) + \frac{\pi F}{\omega}\sin(\varphi) + \frac{2\pi^2\varepsilon_0 R V^2}{\omega A}\left(\frac{D}{\sqrt{D^2 - A^2}} - 1\right) = 0, \tag{A11}$$

$$\frac{\partial S}{\partial \varphi} = \frac{\pi F}{\omega}A\cos(\varphi) - \frac{\pi m \omega_0}{Q}A^2 = 0, \tag{A12}$$

where the underlined variables are calculated along the physical path: $\underline{A}=A$ and $\underline{\varphi}=\varphi$. Introducing the reduced variables, $Z=QF/k$, $m=k/\omega_0^2$, $a_1=A/Z$, $d=D/Z$, and $u=\omega/\omega_0$ gives the system

$$Qa_1(u^2 - 1) + \sin(\varphi) + \frac{2\pi\varepsilon_0 Q R V^2}{kZ^2 a_1}\left(\frac{d}{\sqrt{d^2 - a_1^2}} - 1\right) = 0, \tag{A13}$$

$$\cos(\varphi) - ua_1 = 0, \tag{A14}$$

which is identical to expressions (24) and (22).

The deduction given in this appendix is longer than the development in the Fourier series, given in the text, and therefore not recommended. However, it was useful to demonstrate that the two methods (variational and Fourier) are strictly identical for our system, and that they both neglected the constant deflection z_0 in expression (4) and the corresponding A_0 term omitted in expression (A4).

*FAX: 33 (0)4 67 52 15 84. Email address: leveque@lain.univ-montp2.fr

[1] F. J. Giessibl, Science **267**, 68 (1995).
[2] Y. Sugawara, M. Ohta, H. Ueyama, S. Morita, F. Osaka, S. Ohkouchi, M. Suzuki, and S. Mishima, J. Vac. Sci. Technol. B **B14**, 953 (1996).
[3] S. Kitamura, K. Suzuki, and M. Iwatsuki, Appl. Surf. Sci. **140**, 265 (1999).
[4] S. Morita, M. Abe, K. Tokoyama, and Y. Sugawara, J. Cryst. Growth **210**, 408 (2000).
[5] R. Perez, I. Stich, M. Payne, and K. Terakura, Appl. Surf. Sci. **140**, 320 (1999).
[6] N. Sasaki and M. Tsukuda, Jpn. J. Appl. Phys., Part 1 **38**, 192 (1999).
[7] H. Tang, X. Bouju, C. Joachim, C. Girard, and J. Devillers, J. Chem. Phys. **108**, 359 (1998).
[8] R. Bennewitz, A. S. Foster, L. N. Kantorovich, M. Bammerlin, Ch. Loppacher, S. Schar, M. Guggisberg, E. Meyer, and A. L. Shluger, Phys. Rev. B **62**, 2074 (2000).
[9] A. L. Shluger, A. I. Livshits, A. S. Foster, and C. R. Catlow, J. Phys.: Condens. Matter **11**, R295 (1999).
[10] C. Böhm, F. Saurenbach, P. Taschner, C. Roths, and E. Kubalek, J. Phys. D **26**, 1801 (1993).
[11] M. Tanimoto and O. Vatel, J. Vac. Sci. Technol. B **14**, 1547 (1996).
[12] G. Lévêque, P. Girard, E. Skouri, and D. Yarekha, Appl. Surf. Sci. **157**, 251 (2000).
[13] Y. Yakano, T. Toi, H. Ohno, and K. Yoh, Appl. Surf. Sci. **188**, 399 (2002).
[14] P. Girard, A. N. Titkov, M. Ramonda, V. P. Evtikhiev, and V. P. Ulin, Appl. Surf. Sci. **201**, 1 (2002).
[15] F. J. Giessibl, Phys. Rev. B **56**, 16010 (1997).
[16] J. P. Aimé, G. Couturier, R. Boigard, and L. Nony, Appl. Surf. Sci. **140**, 333 (1999).
[17] L. Nony, R. Boigard, and J. P. Aimé, J. Chem. Phys. **111**, 1615 (1999).
[18] N. Sasaki and M. Tsukada, Appl. Surf. Sci. **140**, 339 (1999).
[19] G. Couturier, L. Nony, R. Boigard, and J. P. Aimé, Appl. Surf. Sci. **188**, 341 (2002).
[20] A. I. Livshits, A. L. Shluger, A. L. Rohl, and A. S. Foster, Phys. Rev. B **59**, 2436 (1999).
[21] S. H. Ke, T. Uda, R. Perez, I. Stich, and K. Terakura, Phys. Rev. B **60**, 11631 (1999).
[22] H. Hölscher, U. Schwarz, and R. Wiesendanger, Appl. Surf. Sci. **140**, 344 (1999).
[23] F. Giessibl, H. Bielefeld, S. Hembacher, and J. Mannhart, Appl. Surf. Sci. **140**, 352 (1999).
[24] R. Dianoux, F. Martins, F. Marchi, C. Alandi, F. Comin, and J. Chevrier, Phys. Rev. B **68**, 045403 (2003).
[25] M. Stark, R. Stark, W. Heckl, and R. Guckenberger, Appl. Phys. Lett. **77**, 3293 (2000).
[26] R. Hillenbrand, M. Stark, and R. Guckenberger, Appl. Phys. Lett. **76**, 3478 (2000).
[27] S. Belaidi, P. Girard, and G. Leveque, J. Appl. Phys. **81**, 1023 (1997).
[28] S. Hudlet, M. Saint Jean, C. Gunthman, and J. Berger, Eur. Phys. J. B **2**, 5 (1998).
[29] T. Albrecht, P. Grütter, D. Horne, and D. Rugar, J. Appl. Phys. **69**, 668 (1991).
[30] B. M. Law and F. Rieutord, Phys. Rev. B **66**, 035402 (2002).
[31] A. Gil, J. Colchero, J. Gomez-Herrero, and A. M. Baro, Nanotechnology **14**, 332 (2003).
[32] J. Cleveland, B. Anczykowski, A. Schmidt, and V. Elings, Appl. Phys. Lett. **72**, 2613 (1998).
[33] J. Tamayo and R. Garcia, Appl. Phys. Lett. **73**, 2926 (1998).
[34] B. Gotsmann, C. Seidel, B. Anczykowski, and H. Fuchs, Phys. Rev. B **60**, 11051 (1999).
[35] B. Anczykowski, D. Krüger, and H. Fuchs, Phys. Rev. B **53**, 15485 (1996).
[36] B. Anczykowski, D. Krüger, K. L. Babcock, and H. Fuchs, Ultramicroscopy **66**, 251 (1996).
[37] R. Garcia and A. San Paulo, Phys. Rev. B **60**, 4961 (1999).
[38] A. San Paulo and R. Garcia, Phys. Rev. B **66** 041406(R) (2002).

[39] R. Garcia and A. San Paulo, Ultramicroscopy **82**, 79 (2000).
[40] M. Marth, D. Maier, J. Honerkamp, R. Brandsch, and G. Bar, J. Appl. Phys. **85**, 7030 (1999).
[41] R. Garcia and A. San Paulo, Phys. Rev. B **61**, R13381 (2000).
[42] H. O. Jacobs, P. Leuchtmann, O. J. Homan, and A. Stemmer, J. Appl. Phys. **84**, 1168 (1998).
[43] H. N. McMurray and G. Williams, J. Appl. Phys. **91**, 1673 (2002).